IEEE Access
Multidisciplinary | Rapid Review | Open Access Journal

Received May 31, 2019, accepted July 2, 2019, date of publication July 12, 2019, date of current version July 31, 2019.

Digital Object Identifier 10.1109/ACCESS.2019.2928421

Empirical Characterization of the Indoor Radio Channel for Array Antenna Systems in the 3 to 4 GHz Frequency Band

JESÚS R. PÉREZ[1], RAFAEL P. TORRES[1], LORENZO RUBIO[2], (Member, IEEE), JOSÉ BASTERRECHEA[1], (Member, IEEE), MARTA DOMINGO[1], VICENT MIQUEL RODRIGO PEÑARROCHA[2], AND JUAN REIG[2], (Member, IEEE)

[1]Department of Communications Engineering, Universidad de Cantabria, 39005 Santander, Spain
[2]Institute of Telecommunications and Multimedia Applications, Universitat Politècnica de València, 46022 Valencia, Spain

Corresponding author: Jesús R. Pérez (jesusramon.perez@unican.es)

This work was supported by the Spanish Ministerio de Economía, Industria y Competitividad under Project TEC2017-86779-C2-1-R and Project TEC2017-86779-C2-2-R.

ABSTRACT Concerning the design and planning of new radio interfaces for the fifth-generation (5G) systems, this paper presents a useful contribution to the characterization of the wideband indoor radio channel in the 3–4-GHz frequency band. A measurement campaign has been carried out in two different indoor scenarios to analyze some of the most important wideband parameters of the propagation channel, including a thorough analysis of its behavior to meet the new radio technology challenges. The channel measurement setup consists of a virtual vertical uniform array at the receiver side of the link that remains at a fixed position, whereas the transmitter side, which is equipped with a single antenna, is placed at different positions in the environment under analysis. The measurement setup emulates the up-link of a multi-user multiple-input multiple-output (MIMO) system and allows obtaining the broadband parameters of the multiple channels that are established between the transmitter and each one of the antennas of the receiver array. The results and conclusions about the path loss, temporal dispersion, and coherence bandwidth are included, along with an analysis of the spatial correlation between wideband channels when one of the antennas is an array.

INDEX TERMS 5G mobile communication, frequency selectivity, massive MIMO, path loss, spatial correlation, temporal dispersion, wideband communications.

I. INTRODUCTION

Since the arrival of the first digital networks to the present day, there has been an unprecedented growth in the demand for mobile services, which is sure to continue and speed up in the next decade. To provide such services and new applications with the required quality, the requirements for future fifth-generation (5G) systems must achieve [1], [2]: an increase in aggregate data rate, with peak speeds that must multiply by a 1000 factor with regard to 4G networks; low latency, less than 1 ms, compared with 10 ms for 4G; and a high mobility, up to 500 km/h.

The aforementioned requirements will require major technological advances, among the most important of which are [1], [2]: (i) ultra-dense cellular networks; (ii) an increase in spectral efficiency by combining beamforming techniques and advanced massive multiple-input multiple-output (MIMO) systems; and above all, (iii) an increase in bandwidth. The increase in the available bandwidth is a key factor and can only be achieved by releasing new bands at higher frequencies.

The mobile industry, academic institutions and international standards-making bodies are trying to determine the most appropriate frequency bands in order to harmonize the use of the spectrum. Currently, there is an agreement that bands that lie in the 3.3 to 4.4 GHz range are the most suitable for the initial 5G deployments and many countries have already reserved those bands to operate the 5G systems. For example, in Europe the 3.4-3.8 GHz band is already allocated to the deployment of such systems and in USA the 3550-3700 MHz band has been allocated for spectrum sharing [3].

The associate editor coordinating the review of this manuscript and approving it for publication was Yejun He.

 This work is licensed under a Creative Commons Attribution 4.0 License. For more information, see http://creativecommons.org/licenses/by/4.0/

Historically, the thorough knowledge of the radio channel has played an important role in the development and deployment of any new generation of mobile systems. Regarding the radio channel models for the 5G systems analysis, they must offer a complete 3D characterization of the channel, including the angular spectra of the departure and arrival directions. However, more usual parameters like the coherence bandwidth and the correlation between channels take on a new relevance in the context of massive MIMO [4], [5].

Over the last two decades, many propagation measurements have been conducted in different environments at frequencies below 6 GHz, e.g., at 900 MHz, 1.7 GHz, 2.4 GHz, 3.5 GHz, 4 GHz, 5.8 GHz, among others [6]–[9], mainly related to cellular communications systems and the deployment of wireless local area networks (WLAN) in the industrial, scientific and medical (ISM) bands. In the case of the 3.5 GHz frequency band, the research activities were initially focused on the characterization of the indoor-to-outdoor (I2O) environments, due to the fact that this band was initially reserved for fixed-to-fixed (F2F) services [10]–[13]. Relatively less attention has been paid to the indoor channel in the 3 to 4 GHz frequency band. In fact, most of the available research activities were focused on the ultra-wideband (UWB) channel characterization from 3.1 to 10.6 GHz [14]–[16]. Moreover, there are several contributions to the indoor channel modeling in this band concerning the polarization effects [17], the time variant modeling of the impulse response [18], [19], along with the contribution of the diffuse scattering to the channel impulse response [20].

The recent interest in the 3.4-3.8 GHz frequency band for the first deployments of future 5G systems has led to the study of the propagation channel characteristics at 3.5 GHz and adjacent bands. In [21], the authors compare the propagation channel characteristics between the 3.5 GHz and 28 GHz frequency bands in an indoor environment. In the framework of the European mmMagic project, the frequency dependency of the radio channel delay spread was investigated from 2 to 86 GHz [22]. The results based on channel measurements in indoor, outdoor and I2O scenarios do not reveal a clear frequency dependency. In contrast, the recent 3GPP TR 38.901 channel model [23] for bands from 0.5 up to 100 GHz has established a frequency dependency in many scenarios. Nevertheless, due to the interest in deploying the first 5G systems in that frequency band, more measurements are required to understand the main characteristics of the propagation channel, especially considering the future use of large arrays at base stations in the framework of multi-user MIMO systems.

This work presents a contribution to the characterization of the indoor channel from 3 to 4 GHz, including the results of a wideband measurement campaign that allows conclusions to be drawn on the path loss, temporal dispersion, frequency selectivity and spatial correlation in MIMO configurations. Section II describes both the measurement system and the measurement environments. Section III presents a discussion of the results achieved and, finally, the main conclusions are outlined in Section IV.

II. MEASUREMENT METHODOLOGY

A. EXPERIMENTAL SETUP

The automated measurement system used to carry out the channel measurements is shown in Fig. 1. The measurement setup consists of a planar scanner along with a E8362A PNA vector network analyzer (VNA), both remote controlled from a computer through RS-232 and general purpose interface bus (GPIB), respectively.

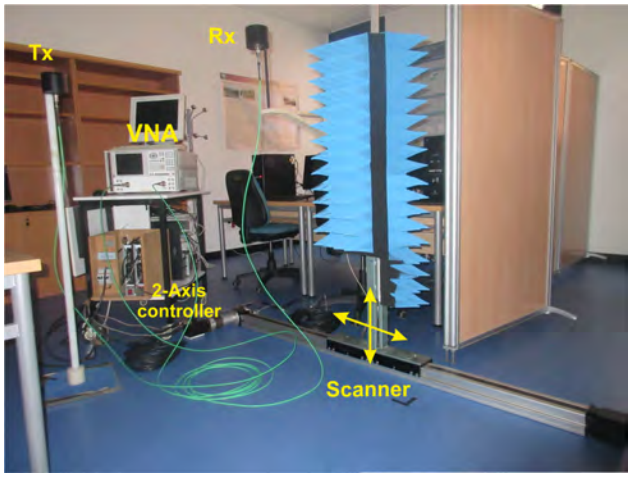

FIGURE 1. Detail of the measurement system.

Regarding the planar scanner, it consists of two servomotors and two linear units, arranged in such a way that the vertical one supports the antenna mast and is fixed on the horizontal one and partially covered with pyramidal absorber material. The scanner allows the user to move the omnidirectional wideband receiver antenna (Rx) on a vertical plane, up to 1.38 m $\times$ 0.81 m in size. At each Rx position, the VNA properly calibrated at both transmitter and receiver radiofrequency cable ends, sends the computer the S_{21}-trace. The post-processing of such information makes it possible to obtain relevant information from the channel.

Concerning the settings considered in this work, the 3 to 4 GHz frequency band has been considered (equivalent to a span of 1 GHz in the VNA), using 801 frequency points (about 1.25 MHz uniformly spaced), resulting in a delay time of 800 ns without aliasing. Furthermore, the transmitter antenna (Tx) is placed on a teflon mast at a height of 1.48 m, and the same height is considered at the center of the scanning area for the Rx. Finally, for any of the Tx positions, the Rx moves on a vertical local area consisting of 7 $\times$ 7 positions ($\lambda/4$ uniformly spaced at 3.5 GHz on both directions, i.e., 21 mm), so this is a virtual vertical uniform rectangular array (URA) with a 1.5λ $\times$ 1.5λ total scanning area.

From a practical point of view, it can be concluded that the measurement system concentrates on the up-link, each

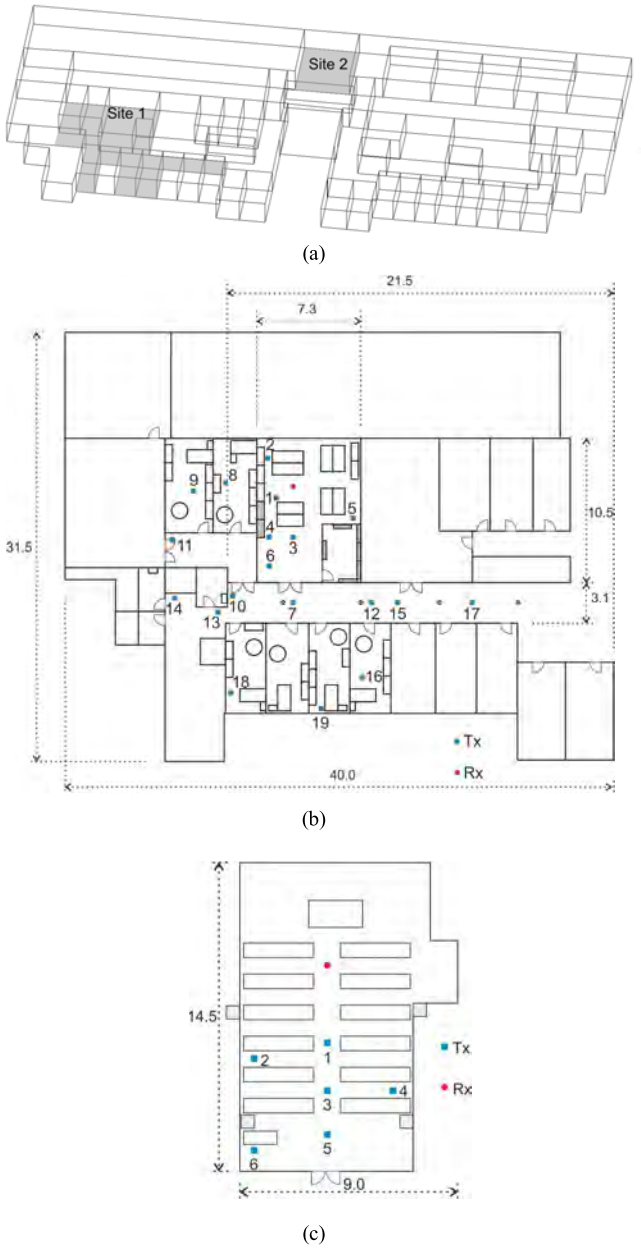

FIGURE 2. Environment with details of Tx and Rx positions, dimensions in meters. (a) 3D-view of the whole floor of the building. (b) Site 1 top view. (c) Site 2 top view.

Tx represents the position of a potential user and the URA a virtual MIMO array at the base station.

B. ENVIRONMENT DESCRIPTION

Measurements have been carried out in two different indoor sites on one of the floors, 93 m × 52 m in size, of the Ingeniería de Telecomunicación "Profesor José Luis García García" building at the University of Cantabria, depicted in Fig. 2(a).

The first scenario is shown in Fig. 2(b) and includes some offices, a long corridor with central columns and a computer laboratory in which the Rx scanner is placed. The laboratory has PC desks and wooden bookshelves as well as metallic bookshelves, the ones shown shadowed in gray. Moreover, Fig. 2(b) also includes the distribution of the office furniture in some nearby offices. The second environment, Site 2 shown in Fig. 2(c), is a meeting room with six rows of desks, a board and chairs.

Regarding the materials of the building, it has indoor drywalls, concrete floors and ceiling boards, concrete columns, as well as metallic doors. It is important to point out that in Site 2 the rear wall consists of a one-meter thick concrete wall and that the Rx is intentionally located between that wall and the metallic front door. Furthermore, to guarantee stationary conditions the measurement campaign has been carried out at night with all the doors closed except for the laboratory's front door.

Finally, as shown in Fig. 2, different Tx positions have been considered in order to analyze the wideband channel parameters in both, line-of-sight (LOS) and non-LOS (NLOS) situations. A total of 19 Tx positions have been measured in Site 1, in LOS and NLOS, and 6 positions in LOS conditions have been measured in Site 2.

III. RESULTS

For the scenarios presented in Fig. 2, this section includes the most representative results obtained in both LOS and NLOS situations. First of all, a detailed analysis of the path loss is presented. Moreover, results concerning the temporal dispersion of the channel and its frequency selectivity are also included and discussed. Finally, interesting results relating the coherence bandwidth and the root-mean-square (RMS) delay spread, as well as an analysis of the spatial correlation of channels between the array elements, are also presented.

A. PATH LOSS

In the case of signals with large bandwidths, larger than the coherence bandwidth of the channel, it is necessary to calculate the path loss taking into account the frequency selectivity of the channel. A generalization of the Friis formula for the case of UWB signals is presented in [24], so for the most general case of an arbitrary propagation environment, an expression to calculate the losses in the frequency domain (FD) can be obtained by using the Parseval's theorem [25]. If we consider that $h[n]$ is the channel impulse response (CIR) measured at the receiver at N temporal samples, we can define the channel path gain (PG), as:

$$PG = \frac{P_r}{P_t} = \sum_{n=0}^{N-1} |h[n]|^2 = \frac{1}{N} \sum_{k=0}^{N-1} |H[k]|^2, \quad (1)$$

where P_r is the received power, P_t is the transmitted power normalized to the unit, and $H[k]$ represents the complex channel transfer function (CTF) at the receiver. According to the measurement and calibration procedure that has been followed, it is verified that:

$$H[k] = S_{21}[k], \quad (2)$$

TABLE 1. Least squares linear regression path loss parameters and 95 % confidence intervals.

Environment	Propagation	γ ($\gamma_{95\%}$)	PL_0 ($PL_{0\,95\%}$)	R^2	σ(dB)
Site 1	LOS	1.81 (1.76-1.86)	41.72 (41.41-42.04)	0.94	1.06
	NLOS	1.69 (1.56-1.82)	54.01 (52.64-55.36)	0.53	2.36
Site 2	LOS	1.15 (1.10-1.19)	47.72 (47.36-48.08)	0.90	0.48

in which $S_{21}[k]$ is the scattering parameter of the k-th frequency tone. The CTF also includes the antenna transfer functions, which depend on their radiation patterns and gains. In order to calculate the path loss, H can be corrected with the gain of the antennas (g_t and g_r), as given in (3):

$$H'[k] = \frac{H[k]}{\sqrt{g_t[k]\, g_r[k]}} = \frac{S_{21}[k]}{\sqrt{g_t[k]\, g_r[k]}}. \tag{3}$$

Finally, the wideband path loss is obtained in the FD by the following expression:

$$\begin{aligned} PL\,(dB) &= 10\log_{10}\left(\frac{1}{PG}\right) \\ &= -10\log_{10}\left(\frac{1}{N}\sum_{k=0}^{N-1}\frac{|S_{21}[k]|^2}{g_t[k]\, g_r[k]}\right), \end{aligned} \tag{4}$$

where N is the number of frequency samples measured.

A commonly accepted path loss model has been considered, so the mean path loss follows a potential law with the distance and the path loss in dB at a distance d between Tx and Rx is given by:

$$PL(d) = PL_0 + 10\,\gamma\,\log_{10}\left(\frac{d}{d_0}\right) + \chi_\sigma, \tag{5}$$

where PL_0 represents the path loss at a reference distance d_0, which is considered equal to 1 m. In addition, γ is the path loss exponent and χ_σ is a random variable with normal distribution, with standard deviation σ, which takes into account the shadow fading, also named shadow factor (SF).

Fig. 3 shows the path loss as a function of the Tx-Rx distance for both Site 1 (Fig. 3(a)) and Site 2 (Fig. 3(b)), representing the values obtained at any of the 49 array measurement points of the receiver URA for every Tx location. Fig. 3(a) includes the losses for both LOS (Tx 1-7) as well as NLOS (Tx 8-19) for well differentiated situations. Moreover, the results in Fig. 3(b) are associated with Tx 1-6, all under LOS condition. Furthermore, Fig. 3 also shows the straight line obtained by the least squares (LS) linear regression fitting of the path loss values as well as the reference wideband free space (WB Free Space) path loss [24]. According to the path loss law given by (5), Table 1 summarizes the parameters obtained by the LS linear regression fitting for both scenarios, the 95% confidence interval, the coefficient of determination, R^2, and the standard deviation or SF, σ.

Focusing on the results at Site 1 and for those Tx-Rx situations under LOS condition, losses are below the WB Free Space value; in fact, a path loss exponent γ lower than 2 is

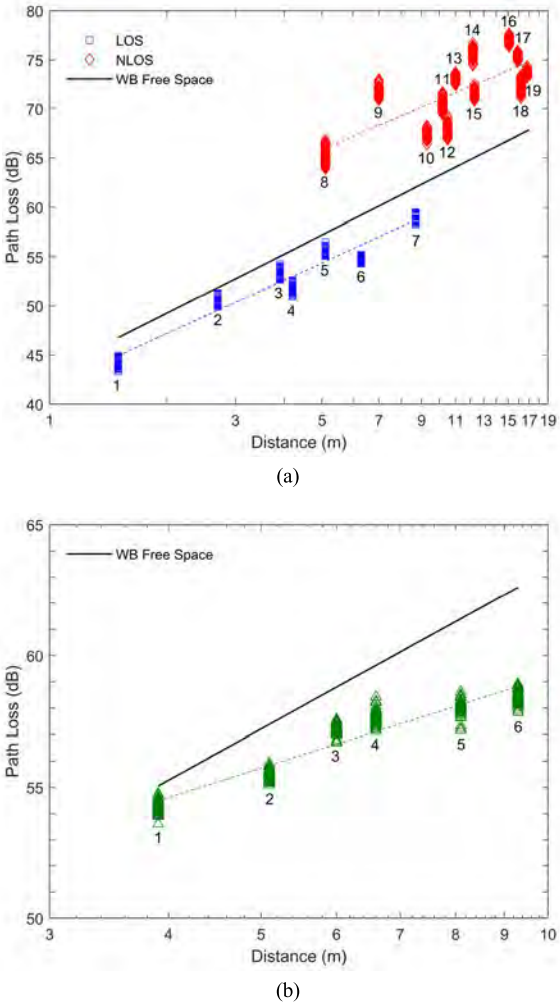

FIGURE 3. Path loss in terms of Tx-Rx distance. (a) Site 1. (b) Site 2.

obtained, similar to other results already reported in the literature for indoor environments in the UWB band [14], [15], and in particular at 3.5 GHz, where a γ of 1.55 has been measured in [21]. Moreover, a coefficient of determination close to one and a narrow 95% confidence interval are obtained. For the NLOS Tx at Site 1, path loss values greater than those obtained in free space are obtained. Despite the fact that γ is also less than 2, the PL_0 value (54.01 dB) is about 12 dB higher than the one obtained in the LOS case.

Furthermore, in the NLOS Tx at Site 1 a lower coefficient of determination (0.53) is obtained which, along with a larger variance of the data, reflect a greater dispersion of

the loss values than in the LOS case. This fact shows that the losses in NLOS situations are more dependent on the specific conditions of propagation than in LOS ones, that is, on the number and characteristics of the elements that obstruct the path between the Tx and Rx. As a comparison with other works, in [21] a path loss exponent of 2.96 was measured in NLOS at 3.5 GHz, but with a lower PL_0 equal to 35.1 dB. Also, a SF equal to 2.8 dB was derived in NLOS, very close to the one obtained here, 2.36 dB.

Regarding Fig. 3(b) and Site 2 LOS results, the path loss values obtained present a different behavior from the ones at Site 1, as the propagation losses decrease very slowly with distance, obtaining a γ of 1.15. This value can be explained by the particular characteristics of this environment. The concrete ceiling and bottom wall as well as the large and metallic front door, give rise to multiple reflections that reach the Rx with high power, resulting in a signal concentration inside the room. These multiple reflections are revealed when analyzing the power delay profile (PDP) and they impact significantly on the RMS delay spread and coherence bandwidth values, as presented in the following subsections.

B. TEMPORAL DISPERSION: RMS DELAY SPREAD

The temporal dispersion caused by the channel over the transmitted signals influences the performance of a wideband communication system. The PDP is the fundamental function from which parameters such as the mean delay and RMS delay spread are calculated. Moreover, the autocorrelation function of the channel in the FD and thus, the frequency selectivity of the channel that is quantified through the coherence bandwidth at different levels of correlation, heavily depend on the aforementioned PDP.

The CIR can be obtained by applying the inverse discrete Fourier transform (IDFT) to the measured transfer function $H[k]$ that consists of 801 equidistant tones on the 1 GHz frequency span. The measured CTF was previously windowed with a Hanning window, $W[k]$ in (6), in order to reduce sidelobe levels prior to obtain the time-domain impulse response. Finally, the PDP is obtained from $h[n]$ as $P[n]= |h[n]|^2$.

$$h[n] = \frac{1}{N}\sum_{k=0}^{N-1} W[k]\, H[k]\, \exp\left(j\frac{2\pi}{N}kn\right). \quad (6)$$

Typical normalized PDP for both Site 1 (LOS and NLOS situations) and Site 2 (LOS) are shown in Fig. 4. At Site 1, from the LOS Tx 3 PDP, the time of arrival of the direct path as well as some reflection components from the walls, ceiling and floor, can be clearly identified; and the maximum excess delay for a threshold (TH) level of 30 dB is 67 ns. Moreover, the NLOS Tx 12 PDP shown in Fig. 4 represents a strong NLOS situation in which the direct path is clearly obstructed. In this case, the contribution associated to the maximum of the PDP is received several ns later than the one associated with the direct path and the maximum excess delay for the 30 dB TH reaches 175 ns, resulting in a more dispersive channel. Finally, the lower graph in Fig. 4 shows the PDP obtained for Tx 5 in Site 2, under LOS conditions.

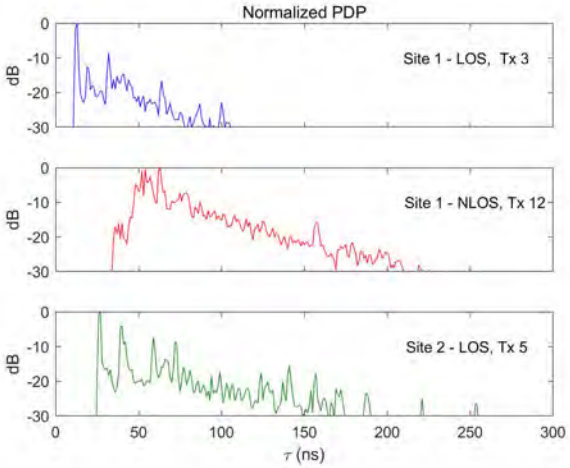

FIGURE 4. Representative power delay profiles for both environments.

As a result of the characteristics already outlined for this particular environment, successive maxima with high power levels can be observed through time. These maxima are clearly identified with the interaction via multiple reflections between the walls, floor, ceiling and the front door. In this case, the maximum excess delay reaches 140 ns, close to the Site 1 Tx 5 NLOS value and more than twice the value obtained for Tx 3 LOS at Site 1; giving rise to a highly dispersive channel.

The RMS delay spread is the statistical parameter obtained from the PDP that best describes the signal dispersion caused by the channel. It is calculated as the square root of the second central moment considering the PDP as a statistical distribution of the power associated with each delay, given as follows [26]:

$$\tau_{RMS} = \sqrt{\frac{\sum_{n=1}^{N} (\tau_n - \bar{\tau})^2\, P[n]}{\sum_{n=1}^{N} P[n]}}, \quad (7)$$

where τ_n is the n-th excess delay time and $\bar{\tau}$ is given by:

$$\bar{\tau} = \frac{\sum_{n=1}^{N} \tau_n\, P[n]}{\sum_{n=1}^{N} P[n]}. \quad (8)$$

Fig. 5 shows the RMS delay spread against distance for both scenarios. In Fig. 5(a), the results for Site 1 including LOS and NLOS values are depicted, and it can be observed that the RMS delay spread values obtained for the NLOS Tx locations undergo a greater dispersion than for the LOS ones. Moreover, Fig. 5(b) shows the results for Site 2 and, despite the fact that all Tx are in LOS locations, it is interesting to note that the RMS delay values are quite high, comparable to those obtained in NLOS at Site 1. This behavior is explained by the multipath richness in this environment, due to its geometric configuration and the lack of furniture. As aforementioned, the PDP for Tx at Site 2 shows how the multiple reflections reach the receiver with broadly high powers even with high delay times.

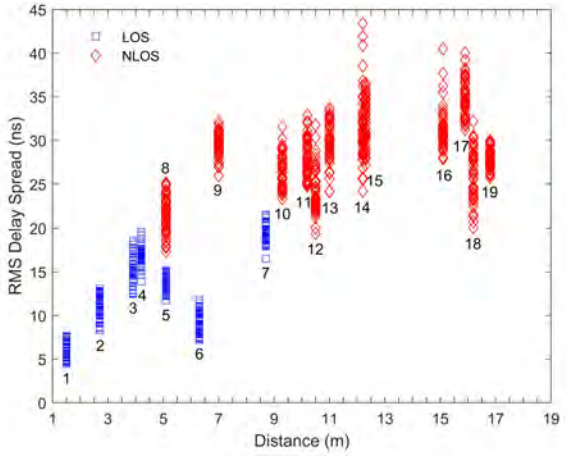

(a)

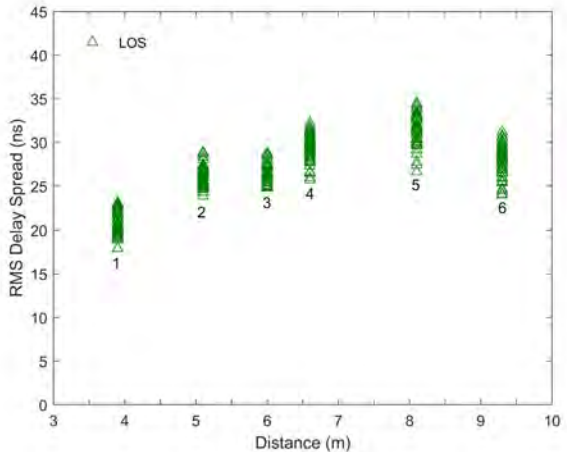

(b)

FIGURE 5. RMS delay spread in terms of Tx-Rx distance. (a) Site 1. (b) Site 2.

A comparison between the overall behavior of the RMS delay spread in LOS and NLOS situations is obtained through the cumulative distribution functions (CDFs) that are shown in Fig. 6. At Site 1 the RMS delay spread varies from 4.5 to 21.5 ns for LOS Tx locations; whereas for the NLOS ones it ranges from 17.3 to 43.4 ns. At Site 2 the RMS delay spread varies from 17.9 to 34.5 ns, a range similar to the NLOS at Site 1. It is worth noting that other results published in the literature show similar differences between LOS and NLOS in frequency bands close to 3 and 4 GHz. Thus, in [8] values of RMS delay spread ranging from 5.4 and 14.9 ns were derived at 2.4 GHz in LOS conditions for indoor office environments, whereas the values in NLOS were higher, ranging from 8.8 to 23.1 ns. In the same indoor environment, the value of RMS delay spread ranges from 7.9 to 18.0 ns and from 10.6 to 23.6 ns at 4.75 GHz in LOS and NLOS conditions, respectively.

In [6] the value of the RMS delay spread oscillates from 22.19 and 30.55 ns in LOS conditions at 2.4 GHz. Nevertheless, the values reported in [21] at 3.5 GHz show no appreciable differences between LOS and NLOS conditions,

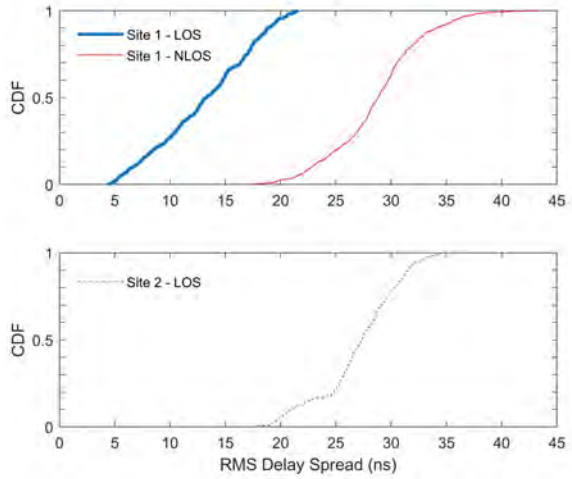

FIGURE 6. CDF of the RMS delay spread for both environments.

and values from 20 up to 70 ns were derived in indoor environments. It is also interesting to highlight that the results reported in [21] establish a growing trend of the RMS delay spread with the distance at 3.5 GHz, in a similar way to the results derived in our work.

C. FREQUENCY SELECTIVITY: COHERENCE BANDWIDTH

The temporal dispersion produced by the channel gives rise to its frequency selectivity. For wide-sense stationary uncorrelated scattering (WSSUS) channels, the frequency correlation function, denoted by $R_{HH}[q]$, can be obtained by means of the Fourier transform of the PDP [26]:

$$R_{HH}[q] = \sum_{n=0}^{N-1} |h[n]|^2 \exp\left(-j\frac{2\pi}{N}nq\right). \quad (9)$$

The correlation function is usually normalized by $\sum_{n=0}^{N-1} |h[n]|^2$ in order to obtain a maximum value of one for the zero lag ($q = 0$). From the correlation function, the coherence bandwidths (B_C) for different correlation levels are obtained [26].

Fig. 7 shows the B_C obtained at Site 1 for both LOS and NLOS locations, and for correlation levels of 0.5, 0.7 and 0.9. For most of the Tx, it can be observed that there is a significant dispersion among the B_C values achieved at the Rx positions inside the URA, although this dispersion is considerably smaller for the B_C (0.9). This fact is common for LOS and NLOS Tx, although the range of variation for the NLOS ones is smaller. Concerning Site 2, Fig. 8 shows the B_C values obtained for the same correlation levels and for the whole set of Tx positions. Again, the results show a great variability of the B_C within the URA, with a range of variation similar to the NLOS case at Site 1.

A global overview of the behavior of the B_C in the measured environments can be obtained through the CDFs. From Fig. 9 and focusing on the CDFs for Site 1, we can observe a usual behavior, so B_C values are always greater for LOS than NLOS locations. Moreover, high B_C values (for any level

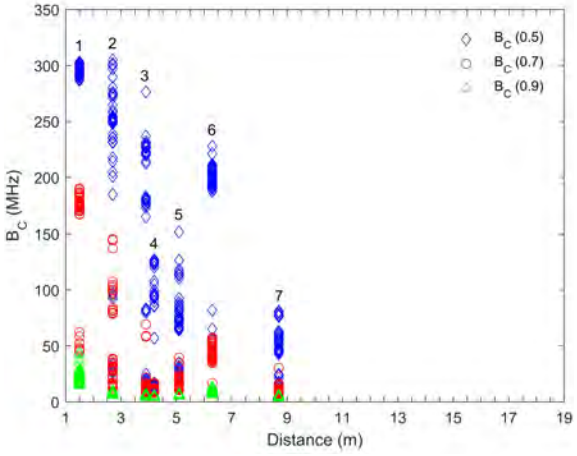

(a)

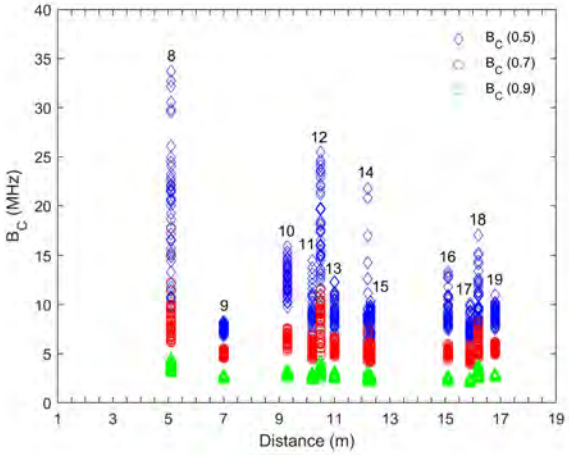

(b)

FIGURE 7. Coherence bandwidth for different correlation levels at Site 1. (a) LOS positions. (b) NLOS positions.

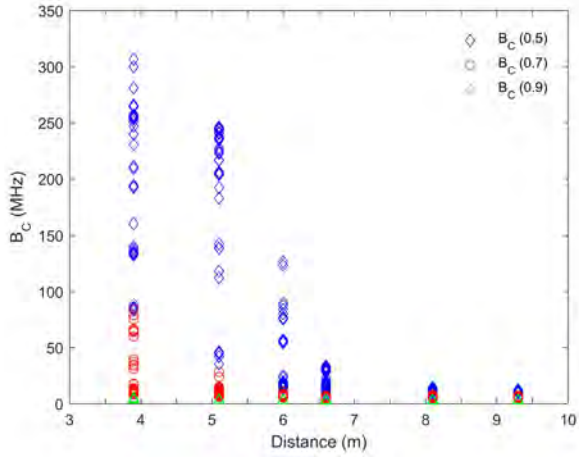

FIGURE 8. Coherence bandwidth for different correlation levels at Site 2.

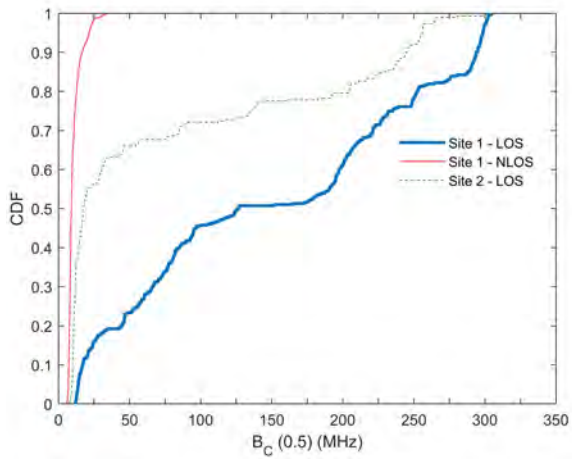

(a)

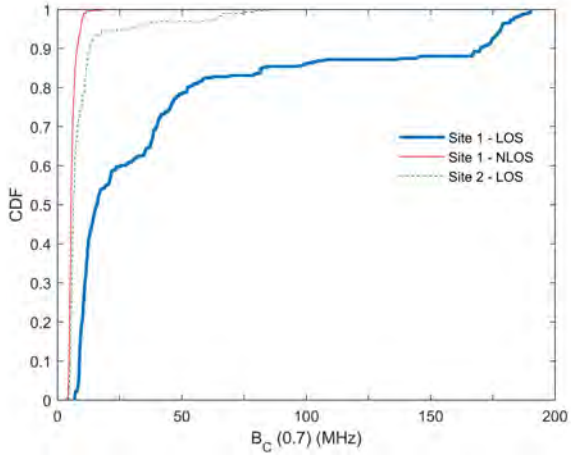

(b)

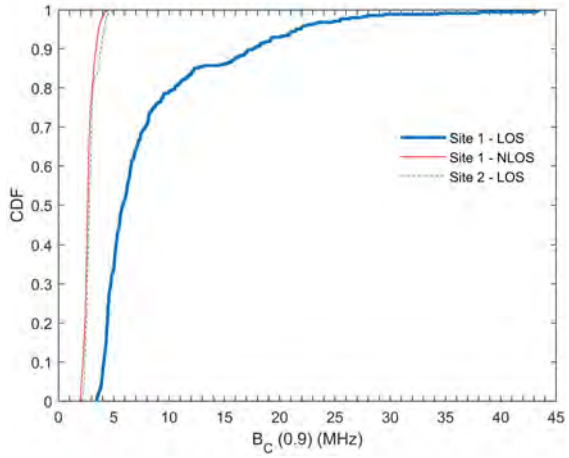

(c)

FIGURE 9. CDF of the coherence bandwidth for both environments and different correlation factors. (a) B_C (0.5). (b) B_C (0.7). (c) B_C (0.9).

of correlation) are also more likely in LOS than in NLOS situations. However, it is important to note that in the lower tails of the CDFs, a convergence occurs, so the B_C values that are exceeded in 90% of locations are relatively close in both situations, LOS and NLOS. For instance, for the representative B_C (0.7), it is observed that the B_C exceeded by 90% is 8.8 MHz for LOS compared to 4.6 MHz

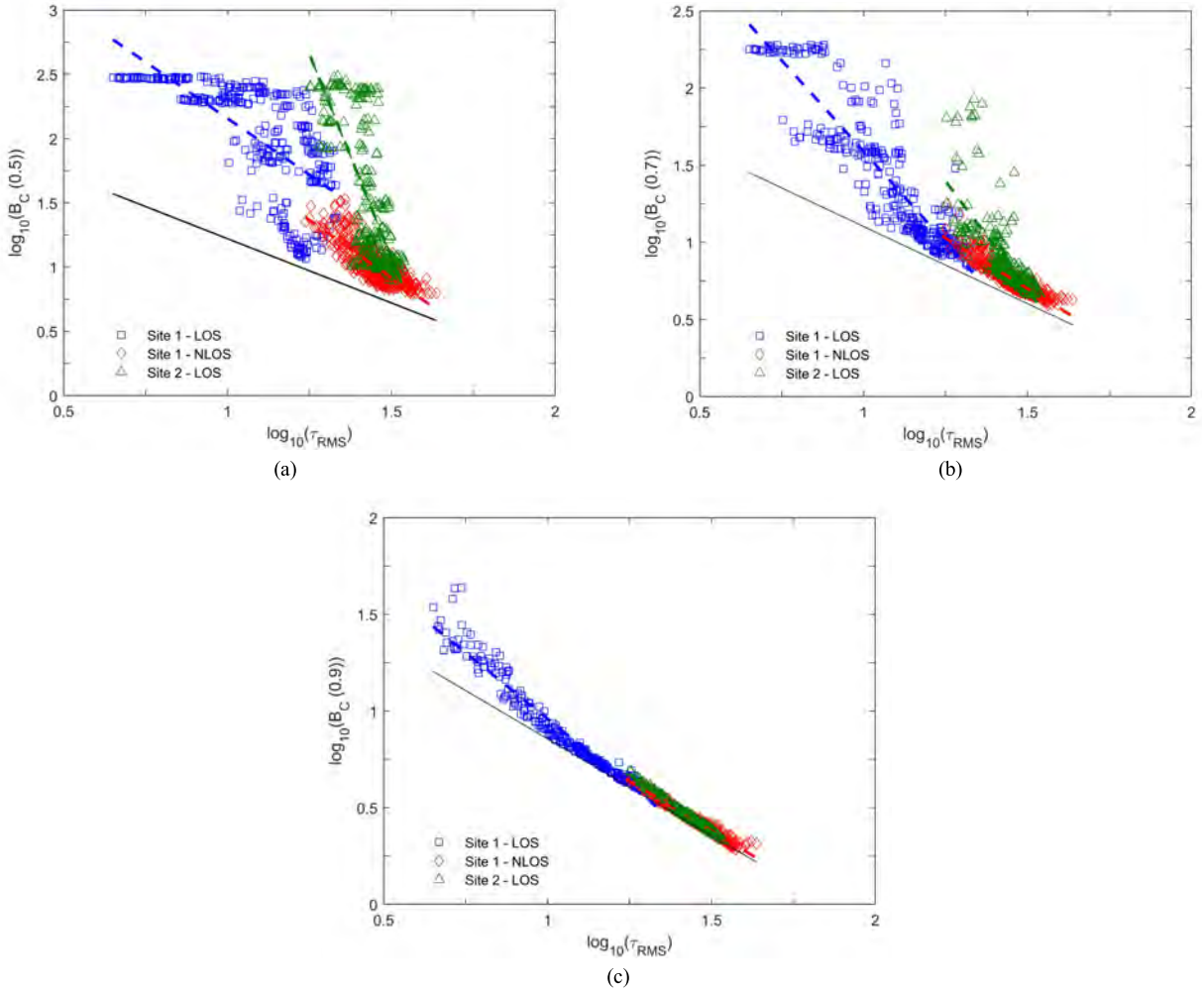

FIGURE 10. Relationship between B_C and τ_{RMS} for both environments and different correlation factors. (a) B_C (0.5). (b) B_C (0.7). (c) B_C (0.9).

for NLOS situations. This fact contrasts with the maximum values achievable in both cases, less than 20 MHz for NLOS in comparison with the 190 MHz for LOS. Regarding Site 2 results, it can be stated that the B_C behavior is between previous LOS and NLOS obtained at Site 1. For instance, for B_C (0.9), the CDF practically coincides with that obtained for NLOS at Site 1. This fact shows that, in indoor environments, the strict classification between LOS and NLOS situations is not as clear as that which occurs outdoors and it makes the specificities of the propagation environment become relevant.

D. RELATIONSHIP BETWEEN B_C AND THE RMS DELAY SPREAD

The relationship between the B_C and the RMS delay spread has both practical as well as theoretical relevance and, in fact, has received a lot of attention since the initial contribution of Gans [27] to the present [28]. The relationship between the PDP and the autocorrelation function through the Fourier transform involves an inverse relationship between the two parameters. Gans proposed a simple relationship, $B_C = 1/\tau_{RMS}$, where the parameter α depends on the shape of the PDP and the degree of correlation that defines B_C [27]. The most significant contributions in order to determine α are summarized in [29].

Fig. 10 shows the results obtained from the measured pairs (τ_{RMS} (ns), B_C(MHz)) at sites 1 and 2 and for the correlation levels considered, i.e., 0.5, 0.7 and 0.9. In [30] a model following the form B_C (MHz) $= \alpha\, \tau_{RMS}^{-\beta}$ (ns) was proposed and, in order to obtain the parameters α and β, a logarithmic transformation of the equation is performed to obtain a linear relationship that was subsequently fitted using LS. Table 2 summarizes the values of the parameters α and β obtained for each site and correlation level.

It can be observed that the determination coefficient for a correlation level of 0.5 takes lower values than for 0.7 and 0.9 levels, concluding that for such a value (0.5) the model does not completely match the relationship between B_C and τ_{RMS}. This fact could be expected just by observing in

TABLE 2. Parameters α, β , their 95 % confidence intervals and the R^2 coefficient.

Environment	Propagation	Correlation level	α ($\alpha_{95\%}$)	β ($\beta_{95\%}$)	R^2
Site 1	LOS	0.5	$8.2{\cdot}10^3$ ($4.9{\cdot}10^3$-$13.7{\cdot}10^3$)	1.75 (1.55-1.96)	0.46
		0.7	$8.9{\cdot}10^3$ ($6.7{\cdot}10^3$-$11.8{\cdot}10^3$)	2.36 (2.25-2.47)	0.83
		0.9	213.32 (197.72-230.12)	1.37 (1.34-1.40)	0.96
	NLOS	0.5	$4.0{\cdot}10^3$ ($2.8{\cdot}10^3$-$5.7{\cdot}10^3$)	1.79 (1.69-1.89)	0.66
		0.7	458.04 (389.04-539.51)	1.31 (1.26-1.36)	0.82
		0.9	83.56 (79.61-87.50)	1.03 (1.01-1.04)	0.97
Site 2	LOS	0.5	$3.8{\cdot}10^{10}$ ($0.4{\cdot}10^{10}$-$38.9{\cdot}10^{10}$)	6.34 (5.63-7.04)	0.52
		0.7	$8.4{\cdot}10^4$ ($3.2{\cdot}10^4$-$22.2{\cdot}10^4$)	2.82 (2.52-3.12)	0.55
		0.9	142.89 (136.14-150.31)	1.19 (1.17-1.20)	0.99

Fig. 10(a) the high dispersion that the measured values of B_C (0.5) exhibit in all the environments. In Fig. 10, Fleury's confinement boundary [31] is also represented using a solid line as a reference, showing that all measured pairs (τ_{RMS}, B_C) are above that boundary, as corresponds with WSSUS channels.

E. SPATIAL CORRELATION OF MULTI-ELEMENT CHANNELS

The measurements of the channel in the 7×7 URA make it possible to obtain the spatial correlation between the 49 existing channels established between the Tx and the 49 Rx positions.

If we consider $H_{pq}[k]$ to be the transfer function of the channel established between the Tx and the (p, q) Rx, then the correlation matrix of the channel will have 49×49 elements calculated as follows,

$$\rho_{pq}^{ij} = \langle H_{pq}, H_{ij} \rangle = \frac{E\left\{H_{pq}H_{ij}^*\right\} - E\left\{H_{pq}\right\}E\left\{H_{ij}^*\right\}}{\sigma_{H_{pq}}\sigma_{H_{ij}}} \quad (10)$$

where $E\{.\}$ is the expected value operating over the frequency, and $\sigma_{H_{pq}}$ is the standard deviation of the (p, q) channel.

Fig. 11 shows two examples of the correlation matrices achieved as a function of the index of antenna position (IoAP), for both a typical LOS as well as a NLOS Tx. In Fig. 11(a), for the LOS case, it is observed how the coefficients of correlation take a value of 1.0 on the diagonal and how they decay as the distance between the Rx increases. Relatively high correlation values are observed: 0.97 for channels associated with antennas located at contiguous positions on the array (λ/4 separated at the central frequency).

Values of correlation lower than 0.7 correspond with antennas separated by more than one wavelength. The comparison with the results obtained in Fig. 11(b) for the NLOS case clearly shows a lower correlation between the channels and a faster reduction of the correlation levels with the distance between the antennas.

To obtain a description of the global behavior of the correlation between antennas in each measurement environment,

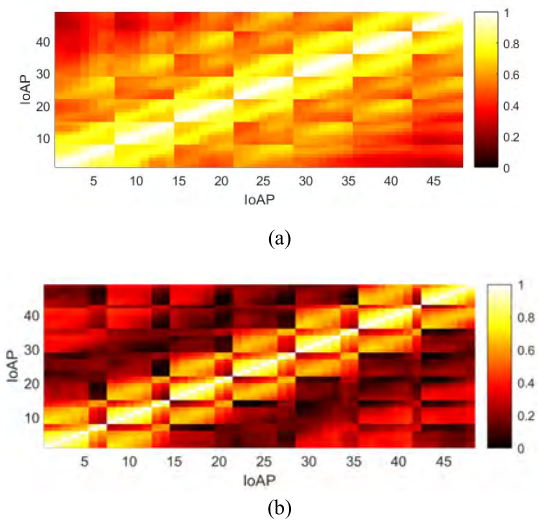

FIGURE 11. Example of correlation matrixes of the 7×7 channels as a function of the IoAP. (a) LOS Tx 4 at Site 2. (b) NLOS Tx 16 at Site 1.

and to be able to have an overall vision of how the correlation changes with the distance between the array antennas, we propose to calculate two mean correlation coefficients: one according to the horizontal coordinate of the array (ρ_H), and the other one on the vertical direction (ρ_V). To calculate ρ_H we take as reference the first antenna of each row of the array and calculate the correlation with the rest of the antennas of its row. This is repeated for each row of the array and we calculate its average value. For the calculation of ρ_V the same procedure is followed by changing rows for columns. Both procedures are mathematically represented by

$$\rho_H(q) = \frac{1}{7}\sum_{p=1}^{7}\langle H_{p,1}, H_{pq}\rangle \quad q = 1, 2, \ldots, 7. \quad (11)$$

$$\rho_V(p) = \frac{1}{7}\sum_{p=1}^{7}\langle H_{1,q}, H_{pq}\rangle \quad p = 1, 2, \ldots, 7. \quad (12)$$

This calculation can be repeated for each Tx at each propagation environment considered. In this sense, Fig. 12 shows the result obtained for both Site 1 (LOS and NLOS) and

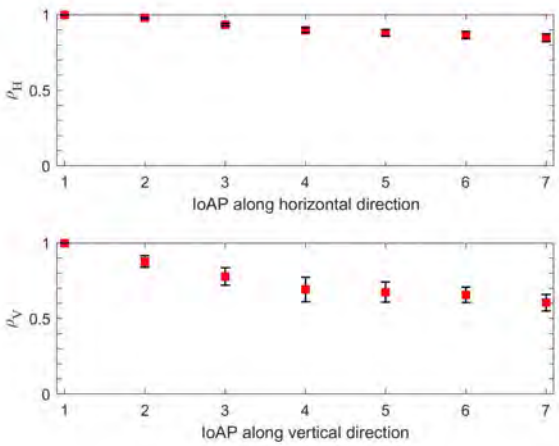

(a)

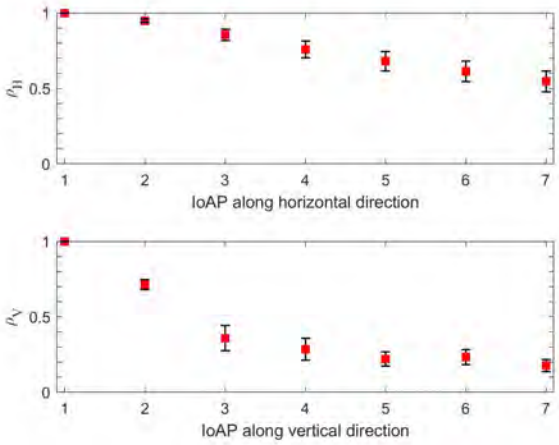

(b)

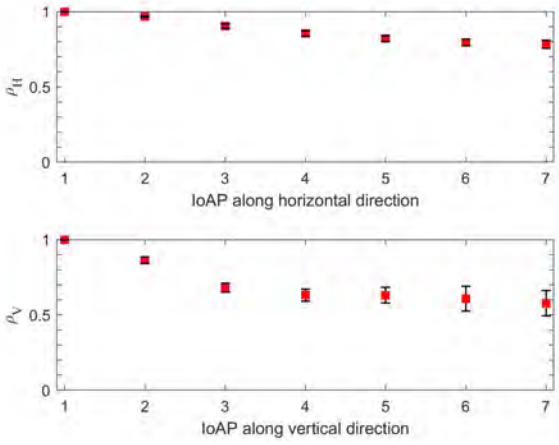

(c)

FIGURE 12. Correlation coefficients of the channels as a function of the loAP in both horizontal and vertical directions. (a) Site 1-LOS. (b) Site 1-NLOS. (c) Site 2-LOS.

Site 2 (LOS). The mean values as well as the standard deviation have been plotted. It can be observed that, in general, the levels of correlation decrease slowly with the distance between antennas, although that decrease is faster when we move along the vertical axis.

If we compare the LOS (Fig. 12(a) and (c)) with the NLOS situations (Fig. 12(b)), it is observed that the correlation decreases more rapidly in the NLOS situations.

If we define the correlation distance as the one from which the mean correlation coefficient drops below a value of 0.7, we can affirm that in the LOS situations this is not practically reached until the end of the array (1.5 λ) for the horizontal direction, being of the order of (λ/2) in the vertical direction. In the NLOS case these distances are of the order of (3λ/4) and (λ/4) for the horizontal and vertical directions respectively. Correlation distances of similar values have been found in indoor environments of similar configurations in nearby frequency bands (2 GHz) [32].

IV. CONCLUSION

The results presented in this paper provide a reference for the design and deployments of future wireless communication systems. From the analysis of the channel measurements, the following conclusions can be drawn:

- Regarding the path loss, the fitting by means of LS of a potential law offers values of the path loss exponents lower than two, in agreement with the values obtained by other authors in nearby frequency bands. A high variance of the data due to shadow fading is observed, especially in NLOS. This dispersion of the path loss values occurs even for the different URA antennas.

- The behavior of the RMS delay spread is different in the two considered environments. In Site 1 the behavior is typical, obtaining lower RMS delay spread values in the LOS positions than in NLOS. However, it is interesting to note that at Site 2 the RMS delay spread varies in a range similar to the NLOS at Site 1. This behavior is explained by the multipath richness that occurs in this environment, due to its geometric configuration and the lack of furniture.

- The coherence bandwidth has been analyzed for different correlation levels. As is usually observed in the literature, the B_C values obtained are always greater for LOS than NLOS locations. However, it is important to note that in the lower tails of the CDFs, a convergence occurs, so the B_C values that are exceeded in 90% of locations are relatively close in both situations, LOS and NLOS.

It is important to notice the great variability that the B_C exhibits in different propagation environments and for the different URA antennas. Taking into account the importance of the B_C in the definition of the time/frequency coherence block in the time division duplex operation (TDD) scheme of massive MIMO systems, which determines the overload due to the estimation of the state of the channel, it will be very important to consider this variability and also determine the degree of coherence necessary to guarantee the efficiency of the signal processing in massive MIMO schemes.

- Regarding the relationship between the RMS delay spread and the coherence bandwidth, the values comply with the theoretical boundary established by Fleury for

WSSUS channels. The relationship in the form $B_C = \alpha\, \tau_{RMS}^{-\beta}$ is largely fulfilled for the coherence bandwidth at the correlation level of 0.9, obtaining a good fit of the experimental values with the proposed model. As the level of correlation with which we define the coherence bandwidth decreases, i.e., 0.7 and 0.5, the suitability of the model is getting worse due to the large dispersion of the coherence bandwidth values.

- The spatial correlation between the sub-channels that are established between each Tx and the different Rx positions in the URA shows a high correlation distance in both scenarios, especially for LOS situations. It is noticeable that, in the LOS situations and for the horizontal direction, a correlation less than 0.7 is not practically reached until the end of the array (1.5λ). This slow variation of the correlation levels with the distance between array antennas is similar to that found in indoor environments in frequency bands close to 3 and 4 GHz.

To obtain a complete overview of the behavior of the channel for multi-user MIMO systems, it is necessary to determine the degree of orthogonality among the multiple channels established between the different users and array antenna elements. Currently, the authors are working on that line with the data obtained from the measurement campaign here presented.

REFERENCES

[1] J. G. Andrews, S. Buzzi, W. Choi, S. V. Hanly, A. Lozano, A. C. K. Soong, and J. C. Zhang, "What will 5G be?" *IEEE J. Sel. Areas Commun.*, vol. 32, no. 6, pp. 1065–1082, Jun. 2014. doi: 10.1109/JSAC.2014.2328098.

[2] T. E. Bogale and L. B. Le, "Massive MIMO and mmWave for 5G Wireless HetNet: Potential benefits and challenges," *IEEE Veh. Technol. Mag.*, vol. 11, no. 1, pp. 64–75, Mar. 2016. doi: 10.1109/MVT.2015.2496240.

[3] *The Future of IMT in the 3300–4200 MHz Spectrum Range*. Accessed: Mar. 2019. [Online]. Available: https://gsacom.com/paper/future-imt-3300-4200-mhz-frequency-range/

[4] T. L. Marzetta, "Noncooperative cellular wireless with unlimited numbers of base station antennas," *IEEE Trans. Wireless Commun.*, vol. 9, no. 11, pp. 3590–3600, Nov. 2010. doi: 10.1109/TWC.2010.092810.091092.

[5] E. Björnson, E. G. Larsson, and T. L. Marzetta, "Massive MIMO: Ten myths and one critical question," *IEEE Commun. Mag.*, vol. 54, no. 2, pp. 114–123, Feb. 2016.

[6] H. J. Zepernick and T. A. Wysocki, "Multipath channel parameters for the indoor radio at 2.4 GHz ISM band," in *Proc. IEEE 49th Veh. Technol. Conf.*, Houston, TX, USA, May 1999, pp. 190–193.

[7] Z. Blažević, I. Zanchi, and I. Marinović, "Propagation measurements at 2.4 GHz inside a university building and estimation of Saleh-Valenzuela parameters," *J. Commun. Softw. Syst.*, vol. 3, no. 2, pp. 99–107, Jun. 2007. doi: 10.24138/jcomss.v3i2.258.

[8] G. J. M. Janssen, P. A. Stigter, and R. Prasad, "Wideband indoor channel measurements and BER analysis of frequency selective multipath channels at 2.4, 4.75, and 11.5 GHz," *IEEE Trans. Commun.*, vol. 44, no. 10, pp. 1272–1288, Oct. 1996.

[9] D. M. J. Devasirvatham and C. Banerjee, "Radio propagation measurements at 850 MHz, 1.7 GHz and 4 GHz inside two dissimilar office buildings," *Electron. Lett.*, vol. 26, no. 7, pp. 445–447, Mar. 1990. doi: 10.1049/el:19900289.

[10] V. Erceg, *Channel Models for Fixed Wireless Broadband Applications*, Standard IEEE 802.16 Broadband Wireless Access Working Group, Feb. 2001.

[11] O. Fernndez, R. Jaramillo, M. Domingo, L. Valle, and R. P. Torres, "Characterization and modeling of BFWA channels in outdoor–indoor environments," *IEEE Antennas Wireless Propag. Lett.*, vol. 6, pp. 236–239, 2007. doi: 10.1109/LAWP.2007.894151.

[12] R. Jaramillo, O. Fernandez, and R. P. Torres, "Empirical analysis of a 2 × 2 MIMO channel in outdoor-indoor scenarios for BFWA applications," *IEEE Antennas Propag. Mag.*, vol. 48, no. 6, pp. 57–69, Dec. 2006.

[13] O. Fernández, M. Domingo, and R. P. Torres, "Empirical analysis of broadband 2 × 2 MIMO channels in outdoor-indoor scenarios," *IEEE Antennas Propag. Mag.*, vol. 52, no. 6, pp. 55–66, Dec. 2010.

[14] S. S. Ghassemzadeh, R. Jana, C. W. Rice, W. Turin, and V. Tarokh, "A statistical path loss model for in-home UWB channels," in *Proc. IEEE Conf. Ultra Wideband Syst. Technol.*, Baltimore, MD, USA, May 2002, pp. 59–64.

[15] W. Ciccognani, A. Durantini, and D. Cassioli, "Time domain propagation measurements of the UWB indoor channel using PN-sequence in the FCC-compliant band 3.6-6 GHz," *IEEE Trans. Antennas Propag.*, vol. 53, no. 4, pp. 1542–1549, Apr. 2005. doi: 10.1109/TAP.2005.844442.

[16] L. Rubio, J. Reig, H. Fernández, and V. M. Rodrigo-Peñarrocha, "Experimental UWB propagation channel path loss and time-dispersion characterization in a laboratory environment," *Int. J. Antennas Propag.*, vol. 2013, Mar. 2013, Art. no. 350167. doi: 10.1155/2013/350167.

[17] F. Quitin, C. Oestges, F. Horlin, and P. D. Doncker, "Polarization measurements and modeling in indoor NLOS environments," *IEEE Trans. Wireless Commun.*, vol. 9, no. 1, pp. 21–25, Jan. 2010. doi: 10.1109/TWC.2010.01.081144.

[18] E. Vinogradov, W. Joseph, and C. Oestges, "Measurement-based modeling of time-variant fading statistics in indoor peer-to-peer scenarios," *IEEE Trans. Antenna Propag.*, vol. 63, no. 5, pp. 2252–2263, May 2015. doi: 10.1109/TAP.2015.2403412.

[19] E. Vinogradov, A. Bamba, W. Joseph, and C. Oestges, "Physical-statistical modeling of dynamic indoor power delay profiles," *IEEE Trans. Wireless Commun.*, vol. 16, no. 10, pp. 6493–6502, Oct. 2017. doi: 10.1109/TWC.2017.2724034.

[20] F. Mani, F. Quitin, and C. Oestges, "Directional spreads of dense multipath components in indoor environments: Experimental validation of a ray-tracing approach," *IEEE Trans. Antennas Propag.*, vol. 60, no. 7, pp. 3389–3396, Jul. 2012. doi: 10.1109/TAP.2012.2196942.

[21] F. Huang, L. Tian, Y. Zheng, and J. Zhang, "Propagation characteristics of indoor radio channel from 3.5 GHz to 28 GHz," in *Proc. IEEE 84th Veh. Technol. Conf.*, Montreal, QC, Canada, Sep. 2016, pp. 1–5.

[22] S. L. H. Nguyen, J. Medbo, M. Peter, A. Karttunen, K. Haneda, A. Bamba, and R. D'Errico, N. Iqbal, C. Diakhate, and J-M. Conrat, "On the frequency dependency of radio channel's delay spread: Analyses and findings from mmMAGIC multi-frequency channel sounding," in *Proc. 12th Eur. Conf. Antennas Propag.*, London, U.K., 2018, pp. 1–5.

[23] *Study on Channel Model for Frequencies From 0.5 to 100 GHz*, document TR 38.901, Release 15, 3GPP, Jun. 2018.

[24] S. Promwong and J. Takada, "Free space link budget estimation scheme for ultra wideband impulse radio with imperfect antennas," *IEICE Electron. Express*, vol. 1, no. 7, pp. 188–192, Jul. 2004. doi: 10.1587/elex.1.188.

[25] A. F. Molisch, "Modulation formats," in *Wireless Communnication*, 2nd ed. London, U.K.: Wiley, 2011, ch. 11, pp. 188–190.

[26] J. D. Parsons, "Wideband channel characterization," in *The Mobile Radio Propagation Channel*, 2nd ed. London, U.K.: Wiley, 2000, ch. 6, pp. 164–189.

[27] M. J. Gans, "A power-spectral theory of propagation in the mobile-radio environment," *IEEE Trans. Veh. Technol.*, vol. 21, no. 1, pp. 27–38, Feb. 1972.

[28] M. Kim, Y. Konishi, Y. Chang, and J.-I. Takada, "Large scale parameters and double-directional characterization of indoor wideband radio multipath channels at 11 GHz," *IEEE Trans. Antennas Propag.*, vol. 62, no. 1, pp. 430–441, Jan. 2014. doi: 10.1109/TAP.2013.2288633.

[29] M. S. Varela and M. G. Sanchez, "RMS delay and coherence bandwidth measurements in indoor radio channels in the UHF band," *IEEE Trans. Veh. Technol.*, vol. 50, no. 2, pp. 515–525, Mar. 2001.

[30] S. J. Howard and K. Pahlavan, "Measurement and analysis of the indoor radio channel in the frequency domain," *IEEE Trans. Instrum. Meas.*, vol. 39, no. 5, pp. 751–755, Oct. 1990.

[31] B. H. Fleury, "An uncertainty relation for WSS processes and its application to WSSUS systems," *IEEE Trans. Commun.*, vol. 44, no. 12, pp. 1632–1634, Dec. 1996.

[32] O. Fernandez, M. Domingo, and R. P. Torres, "Empirical analysis of the correlation of MIMO channels in indoor scenarios at 2 GHz," *IEE Proc.-Commun.*, vol. 152, no. 1, pp. 82–88, Feb. 2005.

JESÚS R. PÉREZ received the B.Sc., M.Sc., and Ph.D. degrees in telecommunications engineering from the University of Cantabria, Spain, in 1996, 1999, and 2005, respectively, where he joined the Department of Communications Engineering, in 1999. He became an Associate Professor, in 2009. His research interests include computational electromagnetics, antenna measurement techniques, radio propagation, and optimization methods. He was awarded a Graduate Research and a Postdoctoral Grant, in 2002 and 2006, respectively.

RAFAEL P. TORRES received the M.S. degree in physics from the University of Granada, Spain, in 1986, and the Ph.D. degree in telecommunications engineering from the Polytechnic University of Madrid (UPM), in 1990. He became an Associate Professor with the Department of Communication Engineering, University of Cantabria, Spain, in 1990. He coauthored a book about the CG-FFT method and authored several chapters in different books and papers as well as about 80 conference contributions. His current research interests include simulation and measurement techniques for radio-propagation and channel characterization for wireless and mobile communications, as well as the simulation and design of new wireless communications systems.

LORENZO RUBIO received the degree in telecommunication engineering and the Ph.D. degree from the Universitat Politécnica de Valéncia (UPV), Spain, in 1996 and 2004, respectively. In 1996, he joined the Communications Department, UPV, where he is currently a Full Professor of wireless and radio communications. His main research interest includes related to wireless communications. Specific current research topics include radiowave propagation, measurement and mobile time-varying channels modeling in vehicular applications, UWB communication systems, multiple-input and multiple-output (MIMO) systems, equalization techniques in digital wireless systems, and mmWave propagation.

JOSÉ BASTERRECHEA (S'92–M'94) received the M.Sc. and Ph.D. degrees in physics (electronics) from the University of Cantabria, in 1987 and 1992, respectively, where he joined the former Department of Electronics, in 1987, and from 1988 to 1991, he was a National Graduate Research Fellow. He became an Assistant Professor with the Department of Communications Engineering, in 1992, and he earned an Associate Professor Position, in 1995. His research interests include numerical methods, electromagnetic compatibility, antenna measurement techniques and optimization, and synthesis methods.

MARTA DOMINGO received the M.Sc. and Ph.D. degrees in physics (electronics) from the University of Cantabria, in 1989 and 1994, respectively, where she became an Associate Professor with the Department of Communication Engineering. She was involved in several research projects. She has authored several papers and conference contributions. Her research interests include numerical and high-frequency methods, simulation and measurements techniques for radio propagation, and channel characterization for wireless and mobile communications.

VICENT MIQUEL RODRIGO PEÑARROCHA was born in Valencia, Spain, in 1966. He received the M.S. degree in telecommunications engineering from the Universidad Politécnica de Madrid, Spain, in 1990, and the Ph.D. degree in telecommunications engineering from the Universitat Politécnica de Valéncia, Spain, in 2003. He joined the Departamento de Comunicaciones, Universitat Politécnica de Valéncia, in 1991, as a Lecturer. His current interests include radiowave propagation, antenna measurements, instrumentation, virtual instrumentation and laboratories, and any educational activity.

JUAN REIG was born in Alcoy, Spain, in 1969. He received the M.S. and Ph.D. degrees in telecommunications engineering from the Universitat Politécnica de Valéncia, Spain, in 1993 and 2000, respectively. He has been a Faculty Member with the Department of Communications, Universitat Politécnica de Valéncia, since 1994, where he is currently an Associate Professor of Telecommunication Engineering. His research interests include fading theory, diversity, ultra-wide band systems, and vehicular communications in V2V and V2I networks.